Faculté de physique et ingénierie
Université de Strasbourg

master PSA Physique Subatomique Astroparticules

Master Science, Mention Physique
Spécialité Physique Subatomique et Astroparticules

Année universitaire **2021-2022**

**Petros STAVROULAKIS**

# OPTIMISATION OF AN UPGRADE TO THE BELLE II EXPERIMENT'S INNER TRACKER USING SIMULATED $B^0 \to K^0_S \, \pi^+\pi^-\gamma$ DECAYS

Rapport de stage de Master
sous la direction de Christian Finck

01 Mars 2022 au 28 Juillet 2022

IPHC Institut Pluridisciplinaire Hubert CURIEN STRASBOURG

Belle II

**Abstract**

The Belle II experiment provides the ideal environment to study rare decay processes, since its collisions are free of contamination from physical background processes that can overshadow a potential discovery of new physics. This is made possible through the use of highly intense collisions between point-like particles, which result in the production of B mesons, particles whose decay properties are worth studying in order to shed more light on the origins of the observed asymmetry between matter and anti-matter in our Universe. While the ever-increasing intensity of Belle II collisions provides a statistically rich data set, it also poses an experimental challenge to the collaboration, which plans to adapt by upgrading the experiment's innermost subdetector, the vertex detector. This work presents the results of an analysis on the performance of a potential upgrade to the Belle II detector's inner tracker, through the use of a measurement that is based on the decays of B mesons to a specific final state. Besides allowing the inner tracker to continue to operate in the harsh environment created by the increased intensity of collisions, this upgrade is also aimed at improving the sensitivity of Belle II to new physics discoveries.

**Résumé**

L'expérience Belle II offre l'environnement idéal pour l'étude des processus de désintégration rares, en effet les collisions $e^+e^-$ soufrent moins de contamination par des processus physiques dus à des particules non élémentaires. Ces dernières pourraient nuire à toute découverte potentielle de nouvelle physique. L'utilisation de collisions très intenses de particules ponctuelles aboutissent à la production de mésons B, des particules dont les propriétés de désintégration seraient une sonde idéale afin de mieux comprendre les origines de l'asymétrie observée entre matière et antimatière dans notre Univers. Si l'intensité toujours croissante des collisions Belle II permet de collecter un jeu de données jamais atteint, elle pose également un défi expérimental à la collaboration, qui prévoit de s'adapter en améliorant le sous-détecteur le plus interne de l'expérience, le détecteur de vertex. Ce travail présente les résultats d'une analyse sur les performances d'une jouvence potentielle du système de trajectographie interne du détecteur Belle II. L'étude a été réalisée à travers un canal de désintégration spécifique des mésons B. En plus de permettre au détecteur Belle II à fonctionner dans l'environnement difficile dû à l'intensité accrue des collisions, cette jouvence vise également à améliorer la sensibilité de Belle II aux découvertes de la nouvelle physique.

# Acknowledgements

I would first like to thank my supervisor Dr. Christian Finck for his valuable guidance during this research internship. I would also like to express my gratitude to Dr. Isabelle Ripp-Baudot and Pr. Jérôme Baudot for believing in me since the beginning and providing me with insightful feedback all throughout my time working with the Belle II group in IPHC Strasbourg. My sincere thanks goes to Dr. Giulio Dujany for being a constant reminder of how significant it is to be skeptical and to always scrutinise my results. I am also thankful to Dr. Benjamin Schwenker for the time he spent to help me familiarise myself with some of the more technical aspects of working with the Belle II simulation software. A big thanks goes to Dr. Varghese Babu for our interesting discussions and his invaluable input regarding both phenomenological as well as technical aspects of my work. Finally, this work would not have been possible without the financial support I received from the ITI QMat International Graduate School this year.

# Contents

# 1. Introduction

The Standard Model (SM) of Particle Physics, along with General Relativity, are the two most successful physical theories developed in the last century. The technological advancements that took place in recent decades have allowed to experimentally test these theories to an extremely high precision, but there exist several questions that are yet unanswered, such as the nature of dark matter and dark energy as well as the vast difference observed in the abundances of matter and anti-matter in the Universe. These observations support the existence of a so-called new physics beyond the SM[1] and nowadays, they are at the forefront of particle physics research.

Belle II is an experiment based in Japan, that records collisions between electrons ($e^-$) and positrons ($e^+$) that have been accelerated by SuperKEKB, the world's highest intensity particle collider. Belle II is specifically designed to make high precision measurements related to the weak interaction and find new physics beyond the SM, by studying the decay properties of particles called B mesons that are produced in $e^+e^-$ collisions.

Several upgrades to the Belle II detector's inner tracker have been proposed in order to cope with the high hit rate induced by the collision rate that SuperKEKB is planned to reach by the start of the next decade. This report presents the results of a performance analysis of one of those upgrades in the context of a measurement based on the decays of B mesons to a specific final state. Specifically, the efficiency with which the final state is reconstructed and the resolution of particle decay points are used to assess the upgrade's performance.

The work covered in this report was conducted in collaboration with the Belle II group at the Institut Pluridisciplinaire Hubert Curien (IPHC) in Strasbourg. It was part of an internship which took place in the fourth semester of a two-year physics master program of the University of Strasbourg, that is centered around subatomic physics.

The document consists of the following sections: chapter 2 presents the physical context and the motivation behind this study, chapter 3 outlines the analysis around which this research internship is centered, a discussion of the results can be found in chapter 4, while a conclusion and future prospects are given in chapter 5.

# 2. Physical context

## 2.1 The Standard Model of Particle Physics and beyond

The Standard Model (SM) of Particle Physics is a theoretical framework that describes the fundamental interactions between subatomic particles, the elementary building blocks of the Universe. Figure 2.1 presents an overview of the SM in terms of its particle content. According to the SM, matter is composed of spin-$\frac{1}{2}$ particles, also called fermions, but only some of them ($u$, $d$, $e$, $\nu_e$) can be found naturally abundant in the Universe. Anti-matter is also comprised of the same set of fermions, only of opposite quantum numbers (e.g. electric charge). Additionally, the SM describes 3 fundamental interactions between the elementary particles: the electromagnetic, weak and strong interactions as forces mediated by spin-1 particles, also called gauge bosons. This elegant picture is completed by the Brout-Englert-Higgs mechanism, that provides the vector bosons and most of the fermions with their masses, and predicts the existence of a scalar boson, the Higgs boson.

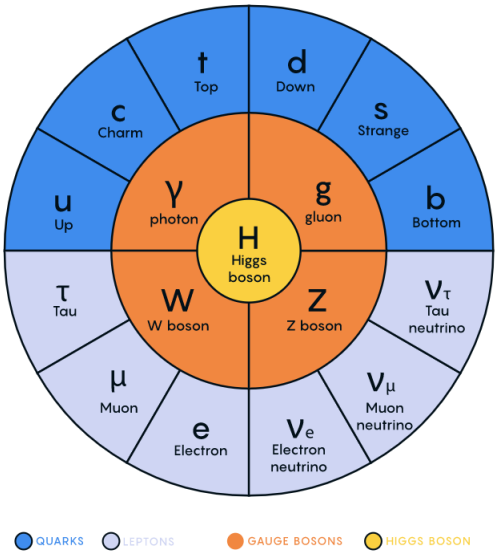


Figure 2.1 – The elementary particles of the SM. It is common to divide matter particles (quarks and leptons) into 3 generations or families, ordered by their masses.

The predictions of the SM have been extensively tested in large-scale particle collider experiments with the last piece of the "puzzle", the Higgs boson, having been discovered in 2012 at the Large Hadron Collider (LHC) at CERN[2]. Despite its triumphs, there exist questions the SM is unable to answer and certain observations that have yet to be explained, such as the origins of the neutrino masses and the rest of the free parameters of the SM, the possibility that more than three generations of particles exist, the nature of dark matter and the origin behind the observed asymmetry between matter and anti-matter in the Universe, to name a few.

Another problem that has come to light in recent years with the increasingly precise measurements performed at particle colliders, are the anomalies observed with processes involving $b \to c$ and $b \to s\ l^+l^-$ quark transitions [1], in that they are observed to occur

1. Here $l^\pm$ stands for charged leptons like $e^\pm, \mu^\pm, \tau^\pm$

more frequently than what is predicted by the SM[3][4]. As such, these transitions are sensitive to contributions from new physics mechanisms not described by the SM, which may provide a sufficient explanation to the observed anomalies. An example of such a transition that is relevant to the work discussed in this report is depicted in Figure 2.2.

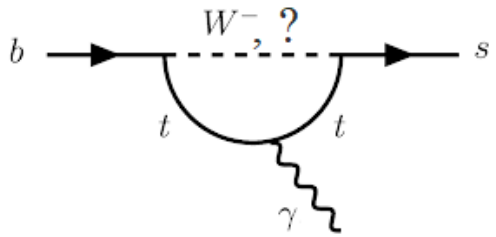


Figure 2.2 – Quark-level $b \to s\,\gamma$ transition that is sensitive to virtual contributions from new particles at the intermediate step of the transition, which is inaccessible directly.

Modern particle physics research seeks answers to such questions at two distinct experimental frontiers:

1. The **Energy Frontier** that seeks to discover new particles by directly detecting them after their manifestation following a highly energetic process. The most recent discovery in this field is the one of the Higgs boson at the LHC at CERN.
2. The **Intensity Frontier** that explores fundamental physics by using intense sources and ultra-sensitive detectors. It encompasses searches for extremely rare processes, like the aforementioned quark transitions, and for significant deviations from Standard Model expectations, that can lead to the discovery of New Physics (NP) mechanisms. An important discovery in this field is that of direct CP violation in the decays of neutral kaons at the Super Proton Synchrotron (SPS) at CERN[5].

The next section will be introducing an experiment that is expected to make significant contributions to the latter frontier, called Belle II.

## 2.2 The Belle II experiment

SuperKEKB is a particle accelerator located in Tsukuba, Japan, which collides beams of electrons and positrons with each other with asymmetric energies ($e^-$ beam: 7 GeV and $e^+$ beam: 4 GeV) at the world's highest instantaneous luminosity, or intensity (current world record: $4.1 \cdot 10^{34}\ cm^{-2}s^{-1}$), and by the start of the next decade, this value will increase by more than an order of magnitude (target: $5 \cdot 10^{35}\ cm^{-2}s^{-1} > 10 \times$ current peak value), as a result of an upgrade to SuperKEKB involving nanometer size beams[6]. The collisions occur at a fixed center-of-mass energy of 10.58 GeV, corresponding to the rest mass energy of the $\Upsilon(4S)$ resonance. The fact that $\Upsilon(4S)$ decays almost immediately to a pair of B mesons more than 96% of the time, is one of two key factors that make SuperKEKB the ideal environment to study their decay properties. The other is the lack of background induced by an underlying event, due to the fact that electrons and positrons are point-like particles and the processes they are allowed to undergo are dictated by their energy, which is known. Another important design feature of SuperKEKB is that its collisions are energetically asymmetric, leading to the $e^+e^-$ system being Lorentz-boosted along the direction of the electron beam. This allows for highly precise measurements to

be performed on important quantities, like lifetimes and CP violation parameters on rare processes, that would be impossible, were it not for this feature[7].

The aftermath of the collisions is recorded by the Belle II detector, displayed in Figure 2.3, a state-of-the-art barrel-shaped spectrometer optimised to detect the various decay products of B mesons. It consists of the following main components, moving outwards from the Interaction Region (IR):

1. The **Vertex Detector (VXD)** made of two layers of DEPFET [2] pixel sensors (PXD) and four layers of double-sided silicon strip sensors (SVD) that measure the decay vertex positions of B mesons and other particles that decay after traveling a short distance.
2. The **Central Drift Chamber (CDC)**, the central tracking device of Belle II, consisting of 56 cylindrical layers of sense wires, placed in a gas volume. A 1.5 T magnetic field permeates the CDC, which is required to measure the momentum of final state charged particles that cross it. The CDC also assists in particle identification through dE/dx measurements.
3. An array of **Time-Of-Propagation (TOP)** counters in the barrel region which, along with the **Aerogel Ring Imaging CHerenkov (A-RICH)** in the end-caps, provide particle identification information.
4. An **Electromagnetic Calorimeter (ECL)** used to reconstruct neutral final state particles, like photons, that deposit their energy in the CsI(Tl) scintillator detectors, forming so-called ECL clusters, which are used to identify them.
5. The **$K_L$-Muon (KLM)**, made of resistive plate chambers that is used to detect $K_L$ and muons ($\mu$).

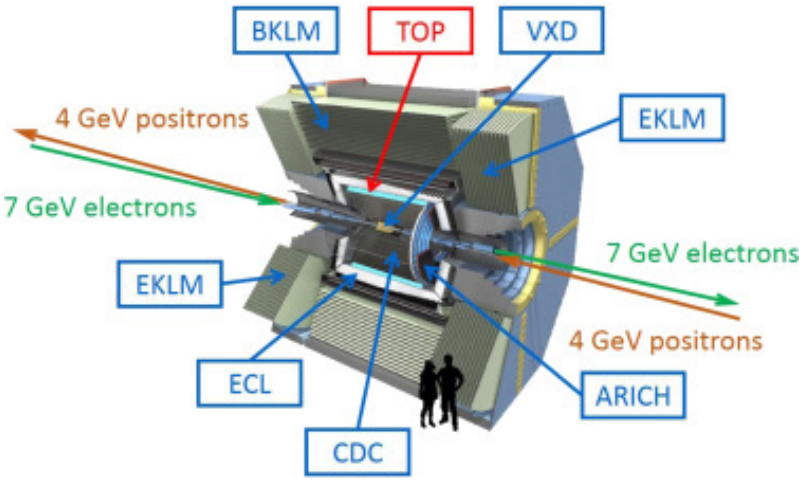


Figure 2.3 – Schematic overview of the Belle II detector and its main components.

More information on the Belle II detector's various components can be found in the Belle II technical design report[8]. The next section describes the problems that arise due to the increased instantaneous luminosity of an upgraded SuperKEKB and how the collaboration plans to address them.

2. DEPleted Field Effect Transistor

## 2.3 Vertex detector upgrade

Since its start in spring 2019, Belle II has accumulated physics data from $e^+e^-$ collisions corresponding to an integrated instantaneous luminosity of 0.4 $ab^{-1}$. This roughly corresponds to a few hundred thousand neutral B mesons produced, out of which only a small fraction participates in rare decays ($\sim 10^{-3}\%$) and is reconstructible ($\sim 5\%$). The aforementioned upgrade to SuperKEKB will further increase the size of the currently available data set to 50 $ab^{-1}$, improving the statistics significantly. However, the increase in instantaneous luminosity that the upgrade will bring, will also lead to more parasite particles being produced by the nano-beams, besides the collision products, called beam background[9]. These parasite particles degrade experimental performances due to increased occupancy in the detector and aging of the detector material. Figure 2.4 shows an expectation for the occupancy levels that will be reached by the inner tracker at the target instantaneous luminosity of Belle II compared to the one of Belle ($\mathcal{L}_{target} \simeq 40 \times \mathcal{L}_{Belle}$ [3]). Were the current vertex detector to operate around the beam intensity of the upgraded SuperKEKB, it will almost certainly not reach the performance standard set by Belle.

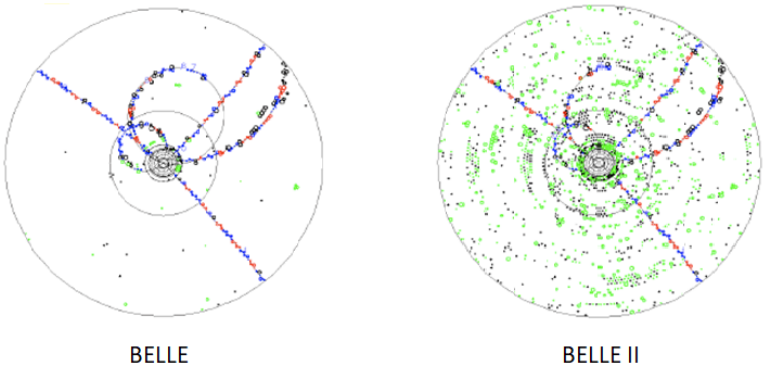


Figure 2.4 – Simulated occupancy levels in Belle and Belle II.

To cope with the increased hit rate, several upgrades to the Belle II vertex detector, the VXD, have been proposed[10]. One such proposal is the VTX project, which replaces the sensors in all layers of the VXD (PXD and SVD) with CMOS [4] pixel sensors. This overall increases the read-out speed and the granularity of the vertex detector, due to the reduced integration time and size of the pixels in the CMOS sensors, respectively. Because of this, detector occupancy is expected to drop by a factor of one thousand ($\sim 0.001\%$) of what the VXD has reached ($\sim 3\%$) with the current luminosity. Actually, at the target instantaneous luminosity, occupancy levels are expected to exceed 100% (3% × 40), so upgrading the VXD is not only beneficial, but necessary. The sensor dedicated to the VTX is called OBELIX and some of its main design features are listed in Table 2.1.

| | |
|---|---|
| Pixel pitch | 30 to 40 $\mu m$ |
| Matrix size | 512 rows × 928 to 752 columns |
| Power dissipation | 100 to 200 $mW/cm^2$ |
| Integration time | 25 to 100 ns |

Table 2.1 – Design characteristics of the OBELIX sensor.

3. Here, $\mathcal{L}$ denotes the instantaneous luminosity
4. Complementary Metal-Oxide Semiconductor

There are currently two layouts of the proposed VTX alongside the current configuration, the VXD, that have been fully implemented in the Belle II analysis software framework (basf2 [5]), on which the analysis discussed in chapter 3 was performed. Regarding the VTX configurations, also called geometries, one consists of five cylindrical coaxial detection layers and the other of seven, both ultimately extending approximately 14 cm away from the IR. All layers in VXD and VTX geometries consist of smaller scale structures, called ladders, on which the sensors are placed. Figure 2.5 shows schematic representations of the VXD and 5 layer VTX geometries and Tables 2.2 and 2.3 list the radii of all the layers and the amount of ladders in each layer together with the amount of sensors in each ladder, respectively, for each of the three detector geometries. By analysing two versions of the upgrade configuration, the goal is to reach a compromise between having a low material budget and an efficient reconstruction of the final state. The following section provides the experimental context needed to motivate the work conducted during this research internship, which is discussed in chapter 3.

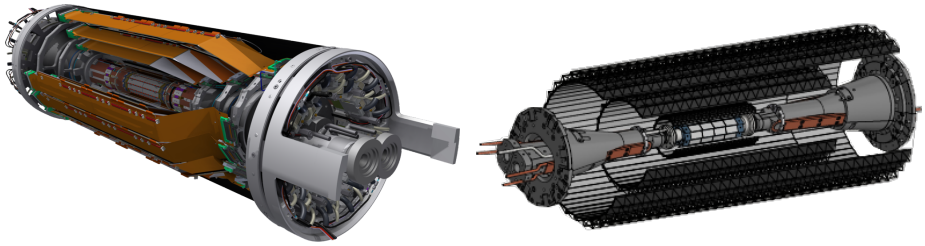

Figure 2.5 – Left: Current vertex detector configuration, the VXD. Right: The VTX configuration with 5 cylindrical detection layers.

| Geometry | Radius (cm) | | | | | | |
|---|---|---|---|---|---|---|---|
| Layer no. | 1 | 2 | 3 | 4 | 5 | 6 | 7 |
| VXD | 1.42 | 2.18 | 3.90 | 8.00 | 10.40 | 13.52 | - |
| VTX 5 layers | 1.41 | 2.21 | 3.91 | 8.95 | 14.00 | - | - |
| VTX 7 layers | 1.41 | 2.21 | 3.51 | 6.01 | 9.01 | 11.50 | 13.50 |

Table 2.2 – Radius of cylindrical layers in each of the 3 detector geometries implemented in basf2.

| Geometry | No. of ladders / No. of sensors per ladder | | | | | | |
|---|---|---|---|---|---|---|---|
| Layer no. | 1 | 2 | 3 | 4 | 5 | 6 | 7 |
| VXD | 8/2 | 12/2 | 7/2 | 10/3 | 12/4 | 16/5 | - |
| VTX 5 layers | 6/4 | 10/4 | 8/8 | 18/16 | 26/24 | - | - |
| VTX 7 layers | 6/4 | 10/4 | 14/8 | 12/12 | 18/16 | 22/20 | 26/24 |

Table 2.3 – No. of ladders per layer and no. of sensors per ladder in each detector geometry (different type of sensor used in VXD and in VTX geometries).

5. For more information on basf2, please visit: software.belle2.org

## 2.4 Time-dependent CP violation in $B^0 \to K^0_S\,\pi^+\pi^-\gamma$ decays

B mesons are composite particles with lifetimes of the order of a trillionth of a second. This makes it challenging to reconstruct B meson pairs that are produced in $e^+e^-$ collisions as separate particles. However, at Belle II events, due to the Lorentz-boost, the B mesons decay far enough apart from each other to make reconstructing them separately possible. Moreover, because no other particles are produced alongside the B meson pair from the decay of the $\Upsilon(4S)$ resonance, the B mesons are quantum entangled and propagate as a superposition of two *mass* states, $B_1$ and $B_2$, until one of the two eventually decays as one of two possible *flavor* states, $B^0$ or anti-$B^0$ ($\overline{B}^0$), and the other B meson travels a distance $\Delta z$ before also decaying. For electrically neutral $B\bar{B}$ pairs, the B meson that decays second can also oscillate between the two flavor states before decaying. This allows to study the mechanism of CP violation especially in the interference[11] between decays of neutral B mesons to a common CP eigenstate $f_{CP}$ directly and after oscillation (i.e. between $B^0 \to f_{CP}$ and $B^0 \to \overline{B}^0 \to f_{CP}$). An illustration of this sequence of events is shown in Figure 2.6.

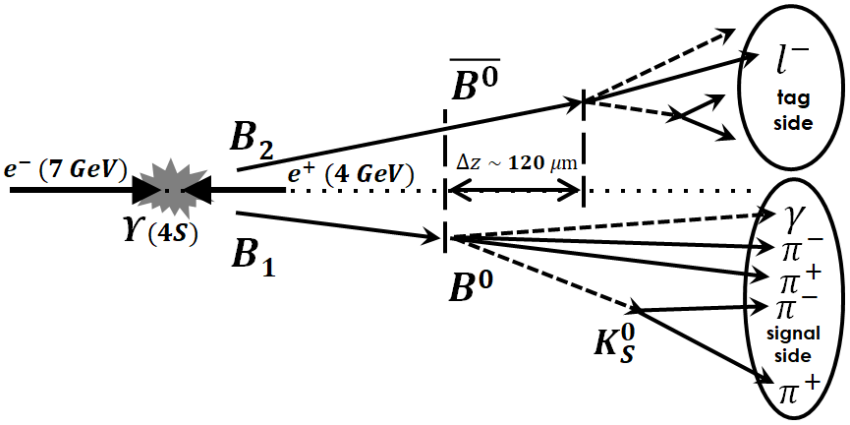


Figure 2.6 – Typical $e^+e^-$ collision resulting in the production of a $B\overline{B}$ pair. The $\Delta t$ resolution is directly proportional to the resolution on the *reconstructed* $\Delta z$.

The observable that is at the center of such studies is called the time-dependent CP asymmetry, defined as:

$$\mathcal{A}_{CP}(\Delta t) \equiv \frac{\Gamma(\overline{B}^0{}_{t=t_0}(\Delta t) \to f_{CP}) - \Gamma(B^0{}_{t=t_0}(\Delta t) \to f_{CP})}{\Gamma(\overline{B}^0{}_{t=t_0}(\Delta t) \to f_{CP}) + \Gamma(B^0{}_{t=t_0}(\Delta t) \to f_{CP})} \tag{2.1}$$

Here, $B^0{}_{t=t_0}(\Delta t)$ and $\overline{B}^0{}_{t=t_0}(\Delta t)$ are the states, which particles identified at time $t = t_0$ as $B^0$ and $\overline{B}^0$ respectively have evolved into, when decaying at time $\Delta t = t - t_0$ to the CP eigenstate $f_{CP}$, while $\Gamma$ denotes the decay rate of the process. Neglecting other sources of CP violation in B meson decays (direct and due to mixing), Equation 2.1 takes the form:

$$\mathcal{A}_{CP}(\Delta t) \simeq S_{f_{CP}} \cdot sin(\Delta m_d \Delta t) \tag{2.2}$$

where $\Delta m_d$ is the mass difference between the two $B^0$ mass eigenstates. The remaining sine term, that arises from the interference between decays of B mesons directly and after $B^0 - \overline{B}^0$ mixing, is parameterised by $S_{f_{CP}}$. In the special case of $B^0$ decays to a $K^0_S$, two charged pions ($\pi^+\pi^-$) and a photon ($\gamma$) like in Figure 2.6, a $b \to s\,\gamma$ transition takes place and, therefore, $\mathcal{A}_{CP}$ becomes highly sensitive to new physics via the circular

polarisation of the final state photon[12]. There are three key factors that can affect the $\mathcal{A}_{CP}$ measurement.

As aforementioned, B mesons have extremely short lifetimes ($\sim$ *psec*), making direct time measurements impossible, even for the world's fastest detectors. Instead, the *resolution* on the time difference $\Delta t$ between the decays of the two B mesons in the event is obtained through measurements of the decay points, or vertices, of the particles, which are conducted by the *vertex detector*. In particular, the longitudinal distance between the two B mesons in an event, $\Delta z$, essentially drives the $\Delta t$ resolution, via the relation $\Delta t = \Delta z/(\beta\gamma\, c)$, where $\beta\gamma$ [6] is a factor that describes the Lorentz boost of the $B\overline{B}$ pair and $c$ is the speed of light.

Aside from the precise knowledge of $\Delta t$, the measurement of the time-dependent CP asymmetry also depends on the quality of *flavor tagging*. Flavor tagging consists of determining the flavor state ($B^0$ or $\overline{B}^0$) of one of the two B mesons at the time of its decay ($t_0$), providing information on the other B meson flavor state, at that same time.

Finally, the measurement of $\mathcal{A}_{CP}$ depends on the *efficiency* with which the final state is reconstructed, which depends on the performance of several detector components, such as the one of the vertex detector, the tracking of the CDC and the calorimeter's reconstruction of neutral particles.

Thus, the $B^0 \to K^0_S\ \pi^+\pi^-\gamma$ decay channel has been chosen as a benchmark for the performance of the proposed VXD upgrade, the VTX, since the final state contains at least 2 charged particle tracks from the $\pi^\pm$ and at least 3 decay vertices in the form of the $K^0_S$ and the 2 $B^0$'s in each event. This, coupled with the fact that $\mathcal{A}_{CP}$ is sensitive to new physics in these decays, motivate the work discussed in the following chapter.

6. In Belle II, $\beta\gamma = 0.284$

# 3. Outline of this work

## 3.1 Simulation and reconstruction of signal events

The goal of this research internship was to compare the performance of the current vertex detector geometry with the ones of the geometries of the proposed upgrade, by specifically examining their ability to reconstruct the particle decay vertices in $B^0 \to K^0_S\, \pi^+\pi^-\gamma$ decays.

The first part of the performance analysis consisted of the simulation and reconstruction of signal events for each of the three available detector geometries (VXD, VTX 5 layer, VTX 7 layer). Specifically, events that contained the decay of a $\mathrm{B}^0$ (or $\overline{\mathrm{B}}^0$) to a $K^0_S\, \pi^+\pi^-\gamma$ final state, with the $\mathrm{K}^0_\mathrm{S}$ also decaying to a pair of charged pions, were generated using the Monte Carlo (MC) simulation tools available in basf2. In total, 40,000 signal events were generated for each geometry, which corresponds to approximately 10 times the number of signal events that exist in the current Belle II data set (0.4 $\mathrm{ab}^{-1}$). Following MC generation, neutral and charged final state particles were simulated [1] in the detector volume and then reconstructed as energy deposits in the electromagnetic calorimeter (ECL) and as tracks in the vertex detector and central drift chamber (CDC), respectively. Alongside the event, physics objects (tracks and ECL clusters) resulting from beam background were also simulated and reconstructed, at the level expected with SuperKEKB operating at the target instantaneous luminosity ($5 \cdot 10^{35}\, cm^{-2}s^{-1}$). Lastly, using the Belle II analysis software tools, the reconstructed objects in the last step were used to reconstruct the decay vertices of the $\mathrm{K}^0_\mathrm{S}$ and $\mathrm{B}^0$ in each event. For the $\mathrm{B}^0$ especially, a set of kinematically justified selection criteria (see Appendix A) was put in place, in order to guarantee a high purity for the reconstructed B meson sample. Moreover, the set of reconstructed $\mathrm{K}^0_\mathrm{S}$'s was limited to the ones originating from $B^0 \to K^0_S\, \pi^+\pi^-\gamma$ decays. This meant $\mathrm{K}^0_\mathrm{S}$'s coming from other $\mathrm{B}^0$ decays were excluded, in order to keep the performance analysis consistent. To exclude such decays, variables that provide information on the generated particles that preceded the $\mathrm{K}^0_\mathrm{S}$ in each event were used.

## 3.2 Quantifying the performance of each detector geometry

The performances of the three geometries were each evaluated on the basis of two main quantities: the reconstruction **efficiency** of $\mathrm{K}^0_\mathrm{S}$'s and $\mathrm{B}^0$'s that belonged to the decay chain of interest ($B^0 \to K^0_S\, \pi^+\pi^-\gamma$), also called *signal* $\mathrm{K}^0_\mathrm{S}$'s and *signal* $\mathrm{B}^0$'s, and the **resolution** on the time difference $\Delta t$ between the decays of the two $\mathrm{B}^0$'s in each event, which itself is derived from the resolution on their decay points (decay vertex resolution).

### 3.2.1 Reconstruction Efficiency

Regarding the reconstruction efficiency, it is defined as the following ratio:

$$\varepsilon_{reco} = \frac{\text{no. of correctly reconstructed candidates}}{\text{no. of generated particles of that type}} \tag{3.1}$$

Several factors contribute to the above formula, such as the efficiency with which individual hits are used to reconstruct tracks, how efficiently particle candidates and decay vertices are reconstructed from those tracks and, finally, the percentage of those candidates and

1. GEANT4 was used to simulate the detector geometry

vertices that actually correspond to generated particles. On the analysis side, computing the efficiency for each geometry amounts to counting the number of particles ($B^0$ and $K^0_S$) that match the corresponding criteria in the numerator and denominator of Equation 3.1, while being consistent with regards to the decay channel. Specifically for the efficiency, more focus was placed on the particles belonging to $B^0 \to K^0_S\, \pi^+\pi^-\gamma$ decays (signal side) than on other decays in the event (tag side), since, as stated in Section 2.4, the ability to reconstruct the final CP eigenstate $f_{CP}$ is a key factor for the successful measurement of the time-dependent CP asymmetry.

To assess the effect of the beam background on it, the reconstruction efficiency of signal $B^0$'s and $K^0_S$'s in the different geometries was calculated both at the nominal level of beam background that is expected at the target instantaneous luminosity and without any beam background.

Lastly, it was also interesting to study how certain quantities like the transverse flight distance or the transverse momentum of $K^0_S$'s can affect whether they were reconstructed or not. Transverse quantities are generally quite useful, because of their potential to reveal important flaws in the detector layout, due to how longitudinally symmetric the vertex detector's geometry is.

### 3.2.2 Decay Vertex Resolution

As for the decay vertex resolution, the process initially involved building the residual [2] distribution of the decay positions of $B^0$'s and $K^0_S$'s for each of the three detector geometries, in order to have a rough estimate of how the resolution is affected by the VTX upgrade.

As was mentioned in Section 2.4, having a high quality measurement of $\Delta t$ (via measuring $\Delta z$) is required in order to make a successful measurement of the time-dependent CP asymmetry, $\mathcal{A}_{CP}$ and, thus, a quantitative method is required to extract the $\Delta t$ resolution, using the $\Delta t$ residual distribution. Specifically, the $\Delta t$ residual distribution was fitted using the sum of 3 Gaussian null-centered distributions, for each one of the three vertex detector geometries, with the resolution value corresponding to the weighted average of the 3 standard deviations obtained from each fit. The following relations were used to extract the resolution values presented in Section 4.2

$$\begin{cases} \sigma_{\Delta t} = \sum_{i=1}^{3} w_i \sigma_i \\ \sigma_{(\sigma_{\Delta t})} = \sqrt{\sum_{i=1}^{3} (w_i \sigma_{\sigma_i})^2} \end{cases} \tag{3.2}$$

where $\sigma_i$ is the standard deviation of the fitted Gaussian distribution, $\sigma_{\sigma_i}$ is the error on $\sigma_i$, $w_i$ is defined as the ratio between the yield of the $i$-th Gaussian over the yield of the sum of the 3 Gaussians and is used to weigh the $\sigma_i$, while $i = 1, 2, 3$ indicates the Gaussian distribution which corresponds to the relevant quantity.

2. difference between true and reconstructed value

# 4. Results and discussion

## 4.1 Reconstruction efficiency

The analysis on the reconstruction of $B^0$'s and $K^0_S$'s discussed in Section 3.2.1 yielded the following results. Figures 4.1 and 4.2 display the efficiency of reconstructing signal $B^0$'s and $K^0_S$'s in the 3 different detector geometries at nominal (BG × 1) and without any (BG × 0) beam background, respectively.

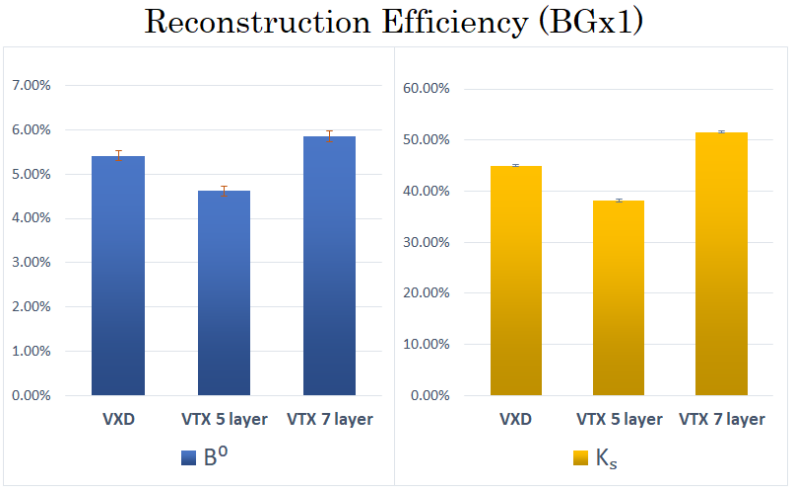


Figure 4.1 – Reconstruction efficiencies at nominal beam background.

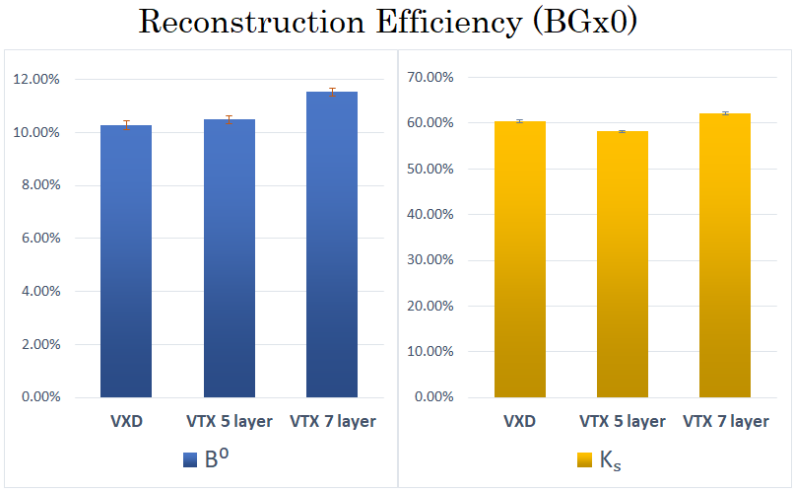


Figure 4.2 – Reconstruction efficiencies at no beam background.

Successful reconstruction of $B^0$'s that participate to $B^0 \to K^0_S\, \pi^+\pi^-\gamma$ decays relies heavily upon reconstructing the $K^0_S$, a process which requires high track reconstruction efficiency, among other things. Indeed, in the more realistic scenario of nominal beam background, the drop in reconstruction efficiency of $K^0_S$'s observed in the 5 layer VTX geometry is significant enough to affect the reconstruction efficiency of $B^0$'s, while, in the case of no beam background, the $B^0$ reconstruction efficiency is overall better in the VTX geometries. Of

course, the rest of the particles in the final state do play an important role in reconstructing the $B^0$, but it is clear from Figure 4.1 that improving $K^0_S$ reconstruction is of greater importance in terms of dealing with the efficiency drop. As for the 7 layer VTX, it outperforms the VXD in reconstruction efficiency, partly due to the higher number of layers, leading to more points available with which to reconstruct charged particle tracks. With regards to single tracks reconstruction, the upgrade geometries have already been proven as more resilient to the higher beam background[13]. As for the drop in efficiency in the 5 layer VTX, it is believed to originate from the unoptimised radial position ($R_{L3} = 3.91$ cm) of the third detection layer in that geometry, which in turn leads to a worse $K^0_S$ reconstruction. This is because $K^0_S$'s may live long enough to decay past that layer, in which case the method that reconstructs the tracks of its daughter particles will have to work using less amount of hits than the amount required to accurately reconstruct them. This conclusion is supported by Figure 4.3 which shows how the reconstruction efficiency of $K^0_S$'s in the VXD and 5 layer VTX geometries changes as a function of the particle's transverse flight distance ($\rho$).

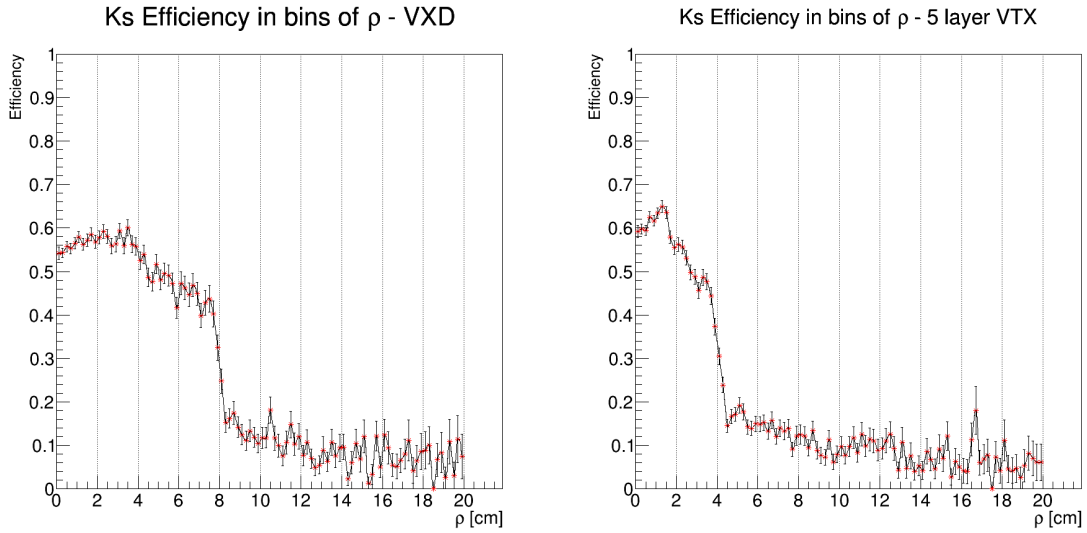


(a) (b)

Figure 4.3 – $K^0_S$ reconstruction efficiency as a function of transverse flight distance in the VXD (left) and 5 layer VTX (right) geometries.

As was expected, shorter lived signal $K^0_S$'s are reconstructed more efficiently in the 5 layer VTX geometry than they are in the VXD, but both start to fail after a certain $K^0_S$ flight distance. As it happens, the transverse flight distance corresponding to the rapid drop in efficiency matches the third to last layer's radial position in both geometries. Looking at Table 2.2, that layer is closer to the beam in the 5 layer VTX than it is in the VXD, and so, the drop in $K^0_S$ reconstruction efficiency appears at shorter flight distances in the former geometry. One way to approach this issue, is to increase the radius of the middle layer in the 5 layer VTX geometry, in order to better reconstruct those longer lived $K^0_S$'s. Another option is to make a 6 layer VTX geometry, by adding an extra layer.

## 4.2 Decay vertex resolution

Regarding the $\Delta t$ resolution, the results of the methodology discussed in Section 3.2.2 are presented in Figure 4.4.

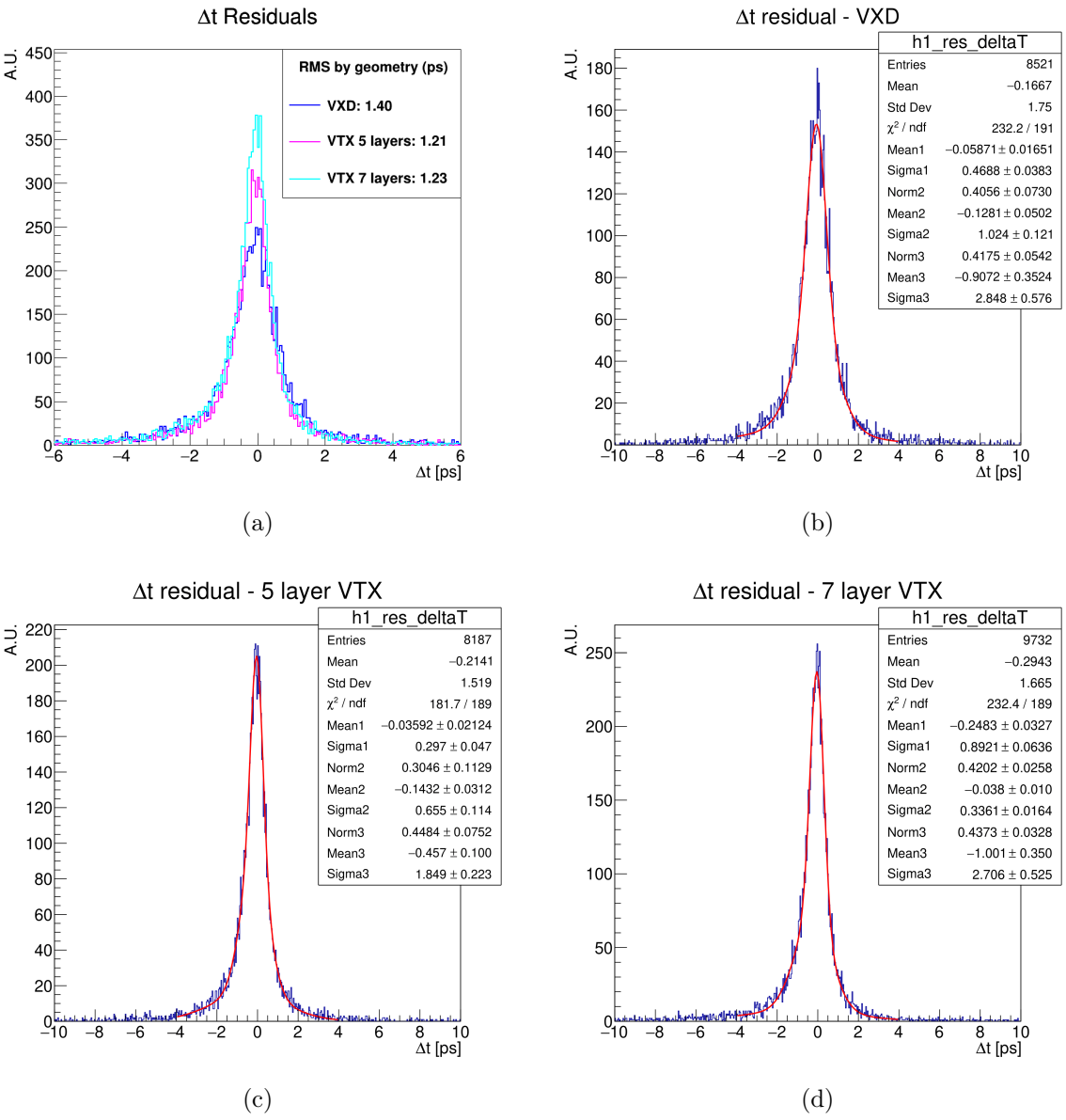


Figure 4.4 – (a): $\Delta t$ residual distributions for all three geometries. (b) – (d): $\Delta t$ residual distributions each fitted using the sum of 3 zero-mean Gaussians. The fit parameters include the mean and standard deviation of each Gaussian (in cm), as well as the fraction of the area under the fit that is covered by the second and third Gaussians.

The resolution values shown in Table 4.1 were obtained, using the parameters extracted from the above fits as inputs to Equations 3.2.

| Geometry | $\Delta t$ resolution (ps) |
|---|---|
| VXD | $1.122 \pm 0.115$ |
| VTX 5 layer | $0.841 \pm 0.077$ |
| VTX 7 layer | $0.907 \pm 0.080$ |

Table 4.1 – $\Delta t$ resolution for the different detector geometries at nominal beam background.

There is a slight ($\sim 2\,\sigma$) improvement in resolution from the VXD to the VTX geometries, partly resulting from the smaller pixel sizes present in the latter case, which leads to an overall better resolution on the reconstructed position of the $B^0$ meson decays. The slight degradation in resolution observed in the 7 layer VTX geometry, with respect to the 5 layer one. is due to the extra material which induces multiple scattering and, as a result, worsens the resolution. In conclusion, in terms of vertex resolution, the VTX manages to reach at least the same performance as the VXD.

As it stands, the VTX geometry that is more realistically planned for implementation is the one with 5 layers, mostly due to mechanical as well as financial reasons. Thus, more focus has been placed in optimising that geometry over the one with 7 layers. To this end, having a more realistic implementation of the 5 layer VTX geometry in the simulation will assist in providing a more accurate picture of its performance. Indeed, the VTX geometries found in the present study, involve sensors that are placed on their respective ladders without any gaps introduced between them and without any passive material. This might lead to false conclusions being drawn from the various performance analyses and, thus, making a more realistic simulation of the VTX is part of the work that follows this research internship.

# 5. Conclusion and outlook

The present work has demonstrated through MC simulations that the proposed vertex detector upgrade, the VTX, manages to cope with the high hit rate induced by the increased instantaneous luminosity while reaching the performance standard set by the VXD operating with the current instantaneous luminosity. The performance of the VTX was assessed on the basis of reconstructing $B^0 \to K^0_S\, \pi^+\pi^-\gamma$ decays and, more precisely, on the efficiency of reconstructing the decay vertices of $\mathrm{B}^0$'s and $\mathrm{K}^0_\mathrm{S}$'s, as well as the resolution on the measured decay positions of $\mathrm{B}^0$'s. It was found that the VTX geometry that consists of 5 layers does not quite reach the reconstruction efficiency of the VXD, while the one with 7 layers is more efficient in reconstructing signal $\mathrm{B}^0$'s and signal $\mathrm{K}^0_\mathrm{S}$'s, at the nominal beam background level. Both VTX geometries were found to be better at resolving $\mathrm{B}^0$ decay positions, and in turn have a slightly better $\Delta t$ resolution, than the VXD. The results of this research internship will be included in the Conceptual Design Report for the upgrade of the Belle II vertex detector and will factor into the collaboration's decision regarding which proposal to eventually implement for the vertex detector upgrade in 2026.

Moving forward, it will be interesting to try to optimise the 5 layer VTX geometry as much as possible, in an attempt to improve its reconstruction capabilities past the ones of the VXD. Moreover, making a more realistic simulation of the 5 layer VTX geometry will assist in providing a more accurate impression of the upgrade's performances. With regards to studying the performances of the VTX geometries that are currently simulated, there are still two highly beneficial analyses to perform. The first of these involves quantifying any possible shifts in the quality of flavor tagging between the current and upgrade vertex detector geometries. The second aspect of the VTX upgrade that has not yet been studied is its robustness against higher levels of beam background than what is expected with the increased instantaneous luminosity of the upgraded SuperKEKB collider.

# Appendices

# A. Selection criteria for signal $B^0$ reconstruction

The criteria used to restrict the sample of reconstructed $B^0$ candidates to ones belonging to $B^0 \to K^0_S\, \pi^+\pi^-\gamma$ decays were:

- At least 5 charged particle tracks present in the event
- $1.4 < E_\gamma < 4.0$ GeV, where $E_\gamma$ is the photon energy
- $|\Delta E| < 0.5$ GeV, where $\Delta E = E_{beam} - E_B$ is the deviation of the nominal beam energy $E_{beam}$ from the reconstructed energy of the B candidate $E_B$
- $5.275 < M_{bc} < 5.29$ GeV/$c^2$, where $M_{bc} = \sqrt{E^2_{beam} - p^2_B}$ is the "beam-constrained mass", with $p_B$ is the momentum magnitude of the B candidate
- $M_{\mathrm{K^0_S}} < 1.533$ GeV/$c^2$, where $M_{\mathrm{K^0_S}}$ is the reconstructed invariant mass of the $K^0_S$ candidate

# B. Complementary plots

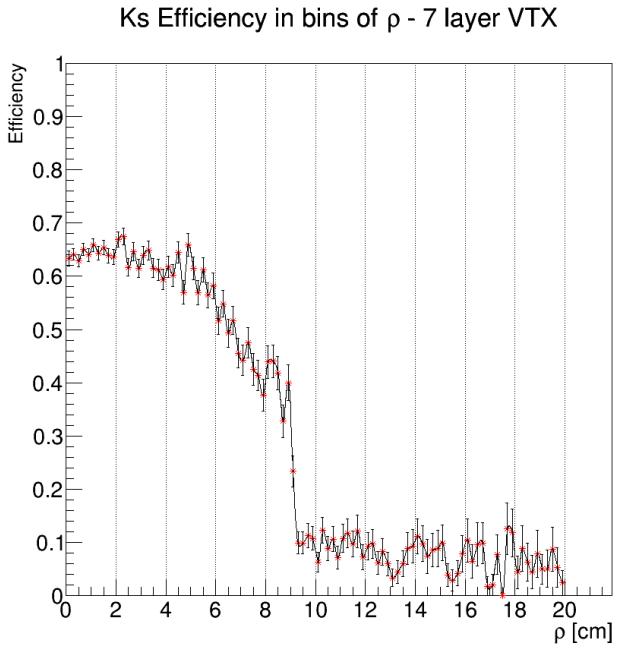


Figure B.1 – $K^0_S$ reconstruction efficiency as a function of transverse flight distance in the 7 layer VTX geometry.

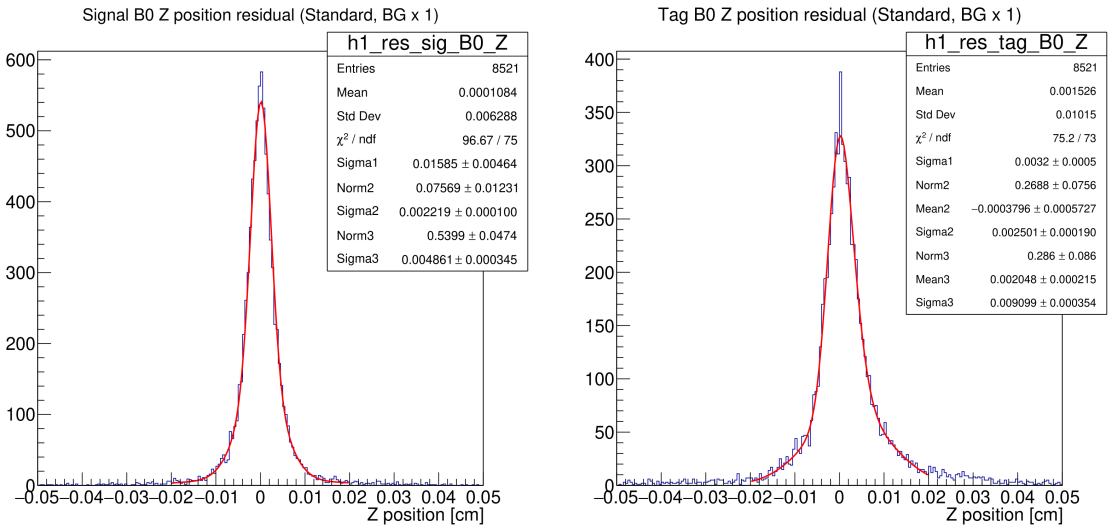


(a) (b)

Figure B.2 – Fitted Z position residual distribution of signal (left) and tag side (right) $B^0$'s in the VXD geometry. For signal $B^0$'s, all Gaussians have their means fixed to 0 and, for tag $B^0$'s, only one out of the 3 has its mean fixed to 0.

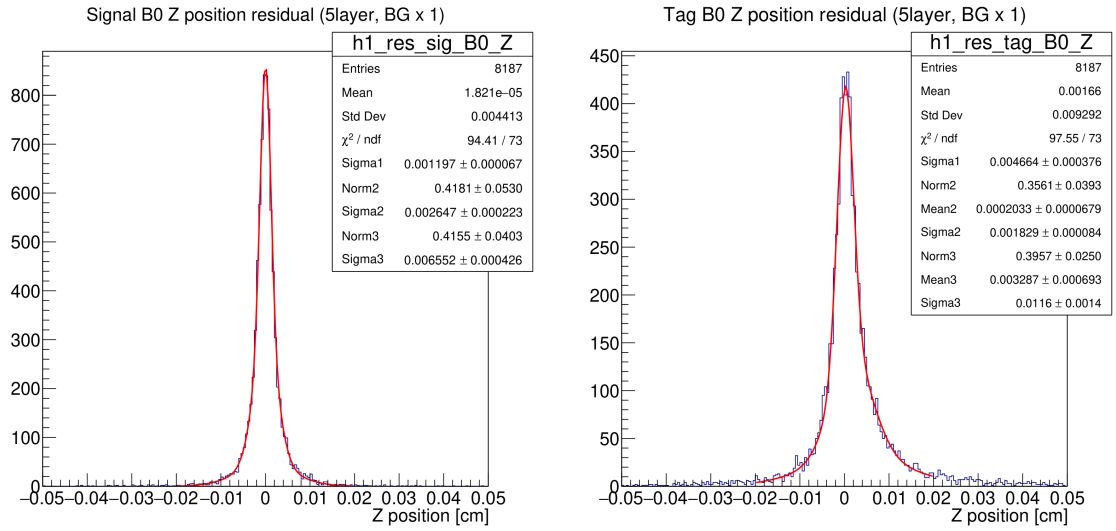


(a) (b)

Figure B.3 – Fitted Z position residual distribution of signal (left) and tag side (right) $B^0$'s in the 5 layer VTX geometry. For signal $B^0$'s, all Gaussians have their means fixed to 0 and, for tag $B^0$'s, only one out of the 3 has its mean fixed to 0.

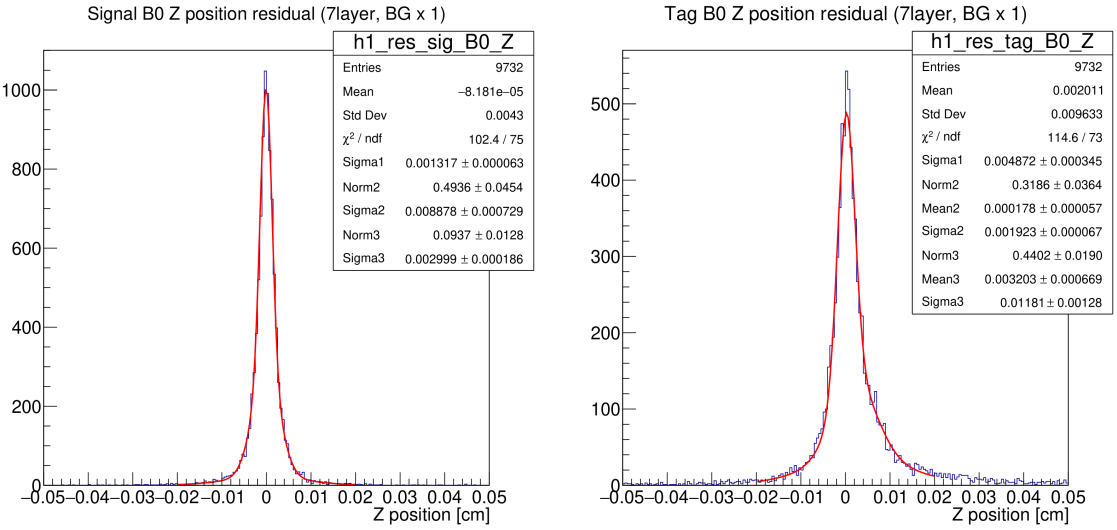


(a) (b)

Figure B.4 – Fitted Z position residual distribution of signal (left) and tag side (right) $B^0$'s in the 7 layer VTX geometry. For signal $B^0$'s, all Gaussians have their means fixed to 0 and, for tag $B^0$'s, only one out of the 3 has its mean fixed to 0.

# Bibliography


[1] J. Ellis. Physics beyond the standard model. *Nuclear Physics A*, 827(1-4):187c–198c, aug 2009. DOI: 10.1016/j.nuclphysa.2009.05.034.

[2] The ATLAS Collaboration. Observation of a new particle in the search for the Standard Model Higgs boson with the ATLAS detector at the LHC. *Physics Letters B*, 716(1):1–29, sep 2012. DOI: 10.1016/j.physletb.2012.08.020.

[3] G. Ciezarek *et al.* A challenge to lepton universality in B-meson decays. *Nature*, 546(7657):227–233, jun 2017. DOI: 10.1038/10.1038/nature22346.

[4] A. Gioventù. $B$-flavour anomalies in $b \to sll$ and $b \to cl\nu_l$ transitions at LHCb. *PoS*, DIS2019:252, 2019. DOI: 10.22323/1.352.0252.

[5] The NA48 Collaboration. Measurment of Direct CP Violation by NA48. In *Multiparticle Dynamics*. World Scientific, mar 2002. DOI: 10.1142/9789812778048_0002.

[6] K. Akai *et al.* SuperKEKB collider. *Nuclear Instruments and Methods in Physics Research Section A*, 907:188–199, 2018. DOI: 10.1016/j.nima.2018.08.017.

[7] E. Kou *et al.* The Belle II Physics Book. *Progress of Theoretical and Experimental Physics*, 2019(12), dec 2019. DOI: 10.1093/ptep/ptz106.

[8] The Belle II Collaboration. Belle II Technical Design Report, 2010. DOI: 10.48550/arxiv.1011.0352.

[9] H. Tanigawa *et al.* Beam background study for the Belle II Silicon Vertex Detector. *Nuclear Instruments and Methods in Physics Research Section A*, 982:164580, 2020. DOI: 10.1016/j.nima.2020.164580.

[10] F. Forti (for the Belle II Collaboration). Snowmass Whitepaper: The Belle II Detector Upgrade Program. *arXiv*, March 2022. DOI: 10.48550/arxiv.2203.11349.

[11] D. Atwood, M. Gronau, and A. Soni. Mixing-Induced CP Asymmetries in Radiative B Decays in and beyond the Standard Model. *Physical Review Letters*, 79(2):185–188, July 1997. DOI: 10.1103/PhysRevLett.79.185.

[12] S. Akar *et al.* The time-dependent *CP* asymmetry in $B^0 \to K_{res}\gamma \to \pi^+\pi^- K_s^0\gamma$ decays. *JHEP*, 2019(9):1–25, 2019. DOI: 10.1007/jhep09(2019)034.

[13] T. Fillinger. Detector Simulation for a Potential Upgrade of the Vertex Detector of the Belle II Experiment. *Acta Phys. Polon. B*, 52(8):909, 2021. DOI: 10.5506/APhysPolB.52.909.